Analysis of nonlinear wave parameters on a rocky shore platform

J. Machado (1) and A.A. Pires-Silva (1)
(1) CERIS, Instituto Superior Técnico, Universidade de Lisboa, Lisbon, Portugal. joaotmachado89@gmail.com

Abstract: The results of a two-day field study conducted on the rocky platform of Ribeira d'Ihas, which is located along the Portuguese western coast, were analysed in order to characterize the wave nonlinearity by calculating the significant wave height to water depth ratio (γ) (breaking and non-breaking sea states), the wave skewness (*Sk*) and the wave asymmetry (*As*).
Higher and lower bound γ values of respectively 1.00 and 0.40 were observed. The γ value increased for a steeper bottom slope. Calculated average values of *Sk* and *As* are of typical surf zone conditions. The increase on the offshore wave energy conditions had an influence on both average values of wave skewness and asymmetry. Furthermore, a steeper bottom slope seemed to reduce both *Sk* and *As*. Also, *Sk* and *As* average values were compared with simulations provided by a wave nonlinearity parameterization *(Ruessink et al., 2012*) which underestimated the wave skewness (~ 25-30%) and asymmetry (~ 50-65%) maximum values. In particular, the wave asymmetry parameterization provided the worst results for the lower local nondimensional parameter *kh*, correspondent to the inner surf zone. The more energetic conditions registered seemed to further compromise *As* simulations in the inner surf zone.

KEYWORDS: Field analysis, Rocky shore platform, Relative wave height, Wave skewness and asymmetry, Parameterizations

1. INTRODUCTION

The hydrodynamic behaviour of wind-generated waves has been extensively addressed on sandy beaches but not so much on rocky platforms. These gently-sloping to near-horizontal rocky surfaces develop seawards and are frequently centred around the mean sea level (MSL).

Sunamura (1992) proposed two generalized rocky shore platform classification types. These types are not distinguished by their bottom slope, but by the existence of a sharp seaward plunging boundary. Type A platforms, usually gently sloping, are characterized by a continuous slope into the nearshore. Type B platforms, frequently near-horizontal, are recognized by having a sharp seaward edge that plunges into the nearshore. In the past few years field studies have been conducted to assess the wave transformation characteristics across rocky platforms (e.g., *Poate et al., 2018*).

Depth induced breaking (or surf breaking) is known to be the most nonlinear and highly dissipative process affecting waves in coastal waters. Entering shallow waters, the wave height (*H*) increases and, with it, so does the wave steepness δ (δ=*H*/*L*, *L* is the wave length). Moreover, the orbital horizontal velocity overcomes the wave celerity, triggering the breaking phenomena (e.g., *Banner and Phillips, 1974*). In this process, nonlinearities in the wave shape develop and linear wave theory no longer holds.

In the surf zone, the significant wave height (H_s) can be approximated by a linearly dependency on water depth (*h*). Hence, establishing a simplified H_s/h relationship can be extremely useful.

The quantification of horizontal and vertical wave shape transformation, both measures of wave nonlinearity, are respectively the wave skewness (*Sk*) and asymmetry (*As*).

Offshore deep water linear sinusoidal waves would have zero values of *Sk* and *As.* As these waves start to change their shape due to shoreward propagation, the *Sk* value reaches its maximum at the breaking point and decreases towards the shoreline. The *As* value steadily decreases (i.e. negative value) shoreward (e.g., *Elgar and Guza, 1985*).

This study aims to analyse and discuss wave nonlinearity across a Type B shore platform and assess its significance in wave transformation into the nearshore. Namely, (breaking and non-breaking) significant relative wave height γ (i.e., the significant wave height to water depth ratio) will be under investigation. Furthermore, nonlinear

wave shape transformation as measures of wave horizontal asymmetry (i.e., *Sk*) and vertical asymmetry (i.e., *As*) will be discussed. Field observations of near-bottom pressure records collected at the intertidal zone of Ribeira d'Ilhas will be analysed for such purpose. Finally, a simple parameterization (*Ruessink et al., 2012*) underpinned on local wave characteristics is to be tested with Ribeira d'Ilhas field data, to assess the extent to which its appliance provides accurate descriptions of wave nonlinearity correspondent to our data.

2. FIELD DATA AND METHODS

2.1 Physical setting

The study site is located along the western Portuguese coastline. Ribeira d'Ilhas is a fully exposed high energy intertidal shore platform (corresponding to Type B of *Sunamura (1992)*) and waves approach predominately from the west-northwest sector. Ribeira d'Ilhas platform and cliff formations developed in near horizontal Lower Cretaceous (Albian) and, concerning its lithology, layers of thick limestones mostly alternate with thin marls (*Andrade et al., 2002*). A 20 to 30 m high cliff, topped by a thick sandstone layer, is fronted by an 80 to 100 m wide rocky shore platform Lower intertidal shore platform is typically near-horizontal with most of its extension lying below the MLWN elevation (i.e., mean low water neap) promoting algal mat setting and growth. Also, sand accumulation takes place upon the upper intertidal RSP surface at low tide, mainly during regular summer months (*Andrade et al., 2002*). Regarding the upper intertidal shore platform site, a high sloping ramp develops landwards, which allows a clear distinction between upper and lower platform boundaries, characterized by differences in both bottom slope (*tan*(*β*)) and roughness and enclosed by the MSL and HHW (i.e., highest high water) elevations.

2.2 Ribeira d'Ilhas campaign

The field campaign was conducted over a two-day period from March 28th to 29th, 2017. Offshore wave buoy (moored at a 500 m depth location) measurements are shown in **Fig.1**.

An almost shore-normal array of 5 pressure transducers (PT) was installed upon the platform surface approximately 5 cm above the bed at the intertidal zone. These PT collected near-bottom pressure records with a sampling frequency (f_s) of 2 Hz. Of note, the landward-most PT (PT5, as PT were numbered from the outer to the inner-most location) was lost during the second day of recordings due to the more energetic wave conditions.

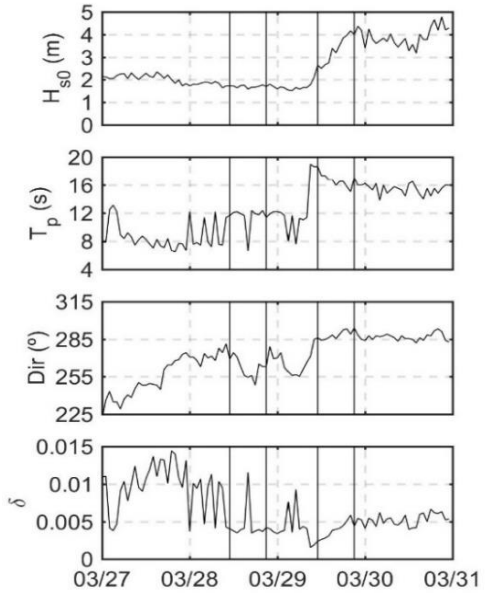

Figure 1 – Offshore wave buoy measurements of significant wave height, peak wave period, frequency integrated mean wave direction and offshore wave steepness from top to bottom, respectively.

Fig.2 illustrates Ribeira d'Ilhas platform cross-shore profile (notice the marked increase in bottom slope (*tan*((*β*)) towards the cliff-foot) with PT deployment positions represented by red crosses.

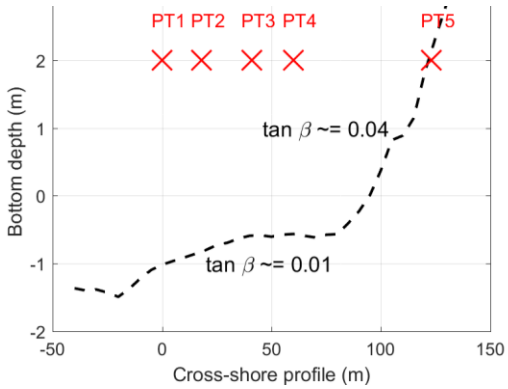

Figure 2 – Ribeira d'Ilhas rocky shore platform cross-shore profile with PT locations identified by red crosses.

2.3 Field data pre-processing

A total of 9 different time series were recorded over the duration of the experiment. Each time series had a total length of approximately 11 hours and was low-pass filtered with a cut-off frequency of 0.001 Hz to remove the tidal oscillations. Next, each time series was divided in 30-minute blocks. The mean value of the tidal

oscillations for each block was defined as *h*. The high-frequency oscillations associated to wind-generated wave motions (η) were obtained by subtracting the tidal oscillations from the original signal.

The wave spectrum ($S(f)$) was computed for each block using the Welch method with 26 degrees of freedom and 0.0039 Hz frequency resolution. A frequency-dependent correction factor was applied based on linear wave theory to take into account the pressure attenuation over the water depth with a maximum correction factor of 4. H_{m0} (or H_s) was obtained through integration of the zeroth spectral moment (m_0) in the short-wave frequency band ($0.04 < f < 0.33$):

$$H_{m0} = H_s = 4\sqrt{\int_{0.04}^{0.33} S(f)\, df} = 4\sqrt{m_0} \quad (1)$$

Once both *h* and H_{m0} were computed for each PT, and for each block, γ was assessed in every PT position. All blocks that had $h < 0.5$ m were excluded from further analysis to remove PT experiencing wet and dry conditions.

2.4 Determination of wave skewness and wave asymmetry

Values of *Sk* and *As* were obtained for each block in every PT location, following *Kennedy et al. (2000)* approach:

$$Sk = \overline{\eta^3} \Big/ \left(\overline{\eta^2}\right)^{3/2} \quad (2)$$

$$As = \overline{\mathcal{H}(\eta^3)} \Big/ \left(\overline{\eta^2}\right)^{3/2} \quad (3)$$

$\mathcal{H}$ in equation (3) represents the Hilbert transform operator and the overbar in (2) and (3) denotes the expected value.

2.5 Ruessink et al.. (2012) parameterization

Values of measured *Sk* and *As* (obtained in the previous section) were compared with the simulations provided by *Ruessink et al. (2012)* parameterizations for both *Sk* and *As*:

$$Sk = Bcos(\psi) \quad (4)$$

$$As = Bsin(\psi) \quad (5)$$

where *B* is the total nonlinearity parameter and ψ is the phase parameter:

$$B = p_1 + \frac{p_2 - p_1}{1 + exp\left(\frac{p_3 - log(Ur)}{p_4}\right)} \quad (6)$$

$$\psi = -\frac{\pi}{2} + \frac{\pi}{2} tanh\left(\frac{p_5}{Ur^{p_6}}\right) \quad (7)$$

where p_1-p_6 consist in non-dimensional parameters and can be used to account for nonlinearity dependence on parameters other than the Ursell number (U_r), which itself consists in a nonlinearity measure based on local wave parameters and depth. Herein, U_r was computed following *Doering and Bowen (1995)*:

$$U_r = \frac{3}{8}\frac{H_s k}{(kh)^3} \quad (8)$$

in which *k* is the wave number ($k=2\pi/L$) and was computed with the linear wave theory using *T* ($T=m_{-1}/m_0$, where m_n is the spectral moment of order *n*). Also, non-dimensional parameters p_1-p_6 used herein were those of *Ruessink et al. (2012)* and come as follows: $p_1=0$, $p_2=0.857\pm0.016$, $p_3=-0.471\pm0.025$, $p_4=0.297\pm0.021$, $p_5=0.815\pm0.055$, $p_6=0.672\pm0.073$ (where the range represented by the ± values is the 95% confidence interval obtained to the data of these authors, hence not applied in this study).

3. RESULTS AND DISCUSSION

3.1 Relationship between significant wave height and water depth

Upper bound γ limits are particularly useful to assess maximum wave conditions that can occur for a given *h*. Concerning the present study, upper bound γ values can be inferred from **Fig.3a** and **3b** (represented by straight lines in both figures) correspondent to day 1 and 2 of the field campaign, respectively. Experiments and studies conducted on sandy beach settings suggested γ to be constant inside the surf zone with an upper bound value of 0.59 (e.g., *Thornton and Guza, 1982*). Moreover, subsequent research works found γ to vary with the offshore wave steepness (e.g., *Nairn et al., 1990*) and with the beach slope (e.g., *Sallenger and Holman, 1985*).

As drawn in **Fig.3a**, an upper bound γ value of 0.40 was observed for the first day data recordings (i.e., black straight line). The landward-most PT (PT5) displayed a higher bound γ value of 1.00 (i.e., red straight line).

This difference is explained by a large increase in the bottom slope towards the cliff-foot. Therefore, the bottom slope contributes to differences in γ values in our study site.
Conversely, in the second day (**Fig.3b**), an upper bound γ value of 0.51 was observed. This slightly higher γ limit may be connected to the 30º change in the offshore (frequency integrated) mean wave direction (**Fig.1**). Note that the offshore wave steepness was approximately similar during the time interval of observations (**Fig.1**).

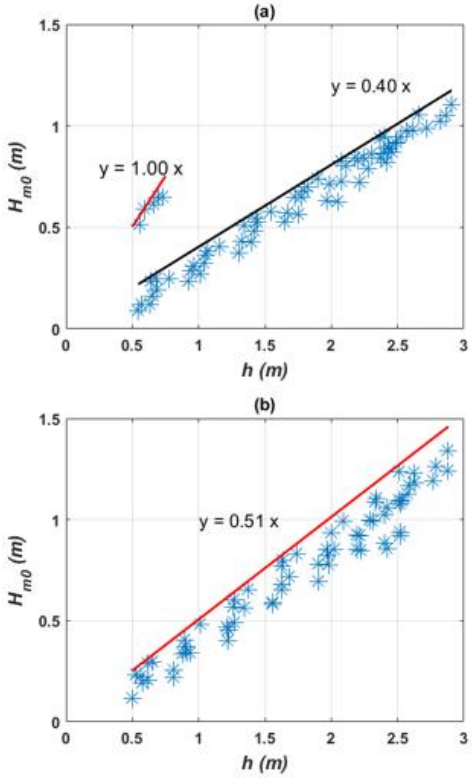

Figure 3 – Significant wave height H_{m0} versus water depth h computed in all PT. Upper bound γ values correspond to the straight lines. a) First day of the field campaign. Red straight line corresponds to the upper bound γ value for the landward-most PT (PT5); Black straight line corresponds to the upper bound γ value associated to the other PT (PT1 to PT4). b) Second day of the field campaign (PT1 to PT4).

Surf zone saturation is observed if H_{m0} shows a linear relationship with *h (Thornton and Guza, 1982*) In addition, *Thornton and Guza (1982)* associated this H_{m0} depth dependence with a high proportion of the waves breaking, being this linear relationship between H_{m0} and *h* that separates the inner surf zone from the outer surf zone. These authors pointed out that the large variability in H_{m0} decreased inside the surf zone. However, a decrease in the variability of H_{m0} was not observed in our study. In fact, the absence of a reduction in H_{m0} variability with water depth suggests that all PT were inside the breaking zone in our study site.

3.2 Wave skewness and asymmetry measured inside the surf zone

Both measures of nonlinear wave shape, namely *Sk* and *As*, were calculated for both days of the field campaign and in each PT position. Results are plotted against *h* in **Fig.4** and **5**.

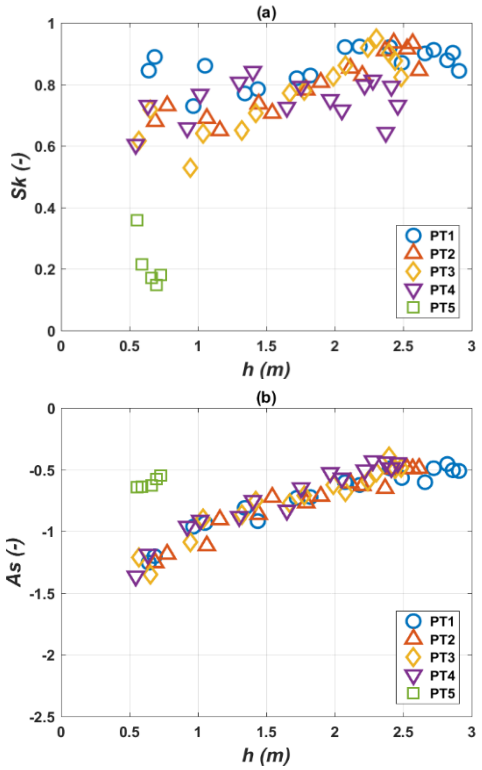

Figure 4 – First day of the field campaign. a) Wave skewness plotted against the water depth in each PT position. b) Wave asymmetry plotted against the water depth in each PT position.

As shown in both **Fig.4** and **5**, the wave shape is not associated to linear sinusoidal waves because both values of *Sk* and *As* were different than zero.

Of interest, the landward-most PT5 (**Fig.4**) showed a considerable decrease of both *Sk* and *As* when compared to the other PT for the same *h*. This may be explained by the effect of the bottom slope in this specific cross-shore location (see **Fig.2**).

Furthermore, it can be seen that for the same *h* differences within both days of the field campaign in terms of *As* and *Sk* were identified.

As an example, *Sk* values were approximately 0.75 for 1.5 m < *h* < 2.0 m in

the first day (**Fig.4a**). For the same *h*, these values dropped to 0.5 in the second day (**Fig.5a**). Since *Sk* values display their maximum near the breaking point and decrease further shoreward, this can be explained by the more energetic offshore wave conditions experienced during the second day (first panel of **Fig.1**). The breakpoint location likely moved seaward and PT were located further inside the surf zone during the second day. Similar changes can be seen for *As* with an increase during the second day.

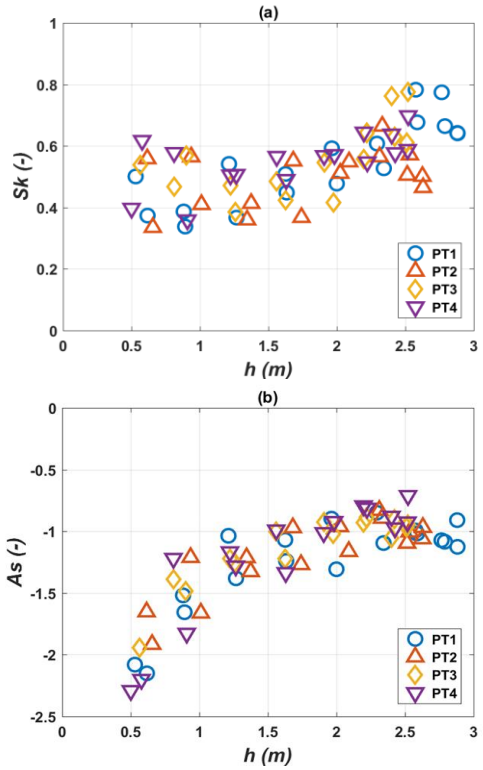

Figure 5 – Second day of the field campaign. a) Wave skewness plotted against the water depth in each PT position. b) Wave asymmetry plotted against the water depth in each PT position.

Both *Sk* and *As* differences are congruent and can be explained by the more energetic conditions registered in the second day. The breaking location probably occurred in a seaward position (when compared to the first day), thereby widening the breaking zone.

Furthermore, both *Sk* and *As* values are similar to those identified in other conducted studies (e.g., *Kennedy et al., 2000*). These values denote highly nonlinear shoaling and breaking waves, meaning continuous and turbulent wave energy dissipation due to depth induced breaking towards the shore.

3.3 Wave skewness and asymmetry simulated inside the surf zone

Both measures of simulated nonlinear wave shape ($Sk_{predicted}$ *and* $As_{predicted}$) were computed for the two days of the field campaign and in each PT position, following *Ruessink et al. (2012)* approach descripted in section ***2.5***. Results where then compared with those obtained from the acquired field data ($Sk_{measured}$ and $As_{measured}$), presented in section ***2.4***. To the purpose of including U_r in the analysis, itself a nonlinearity measure derived from local parameters, results of both measured and simulated nonlinear wave shape where plotted against each other and set to display their respective U_r (**Fig.6**). Once again, all data with h < 0.5 m were removed not to include PT emersion periods (meaning that swash zone data is not included in the analysis). For practical purposes and from now on, *Ruessink et al. (2012)* study will be referred to as "***R12***".

As shown in **Fig.6** (panels (a) and (c)) *Sk* is underestimated by ***R12*** formula. It performs worse in the first day (panel (a)) as $Sk_{predicted}$ significantly underestimates the measured *Sk* values, particularly the highest $Sk_{measured}$. However, in the second day (panel (c)), the trend is a better fit, although with generally lower *Sk* values (and in agreement with the results discussed in the previous section). This suggests a limitation in ***R12*** formulas (**eq. (6)** and **(7)**), regarding the maximum measured *Sk* values (which are likely to have happened near the breaking point, after waves endured substantial shoaling). Notice that the maximum measured *Sk* is underestimated by ~30% and ~25%, respectively in the first (**Fig.6a**) and second (**Fig.6c**) days of the field experiment. Although the ***R12*** formulation performance did not improve much towards the second day of the campaign regarding *Sk* maximum values prediction, it definitely provided a better overall *Sk* description. Moreover, it is interesting to observe that the ***R12*** formula simulates *Sk* behaviour decently in PT5 cross-location (**Fig.6a**). However, care should be taken not only due to the few data points available (with h < 0.5 m) in this specific platform location but also because of the large increase in the bed slope reaching the cliff-foot (see **Fig.2**) (which consists in one of the acknowledged limitations of ***R12*** parameterization.

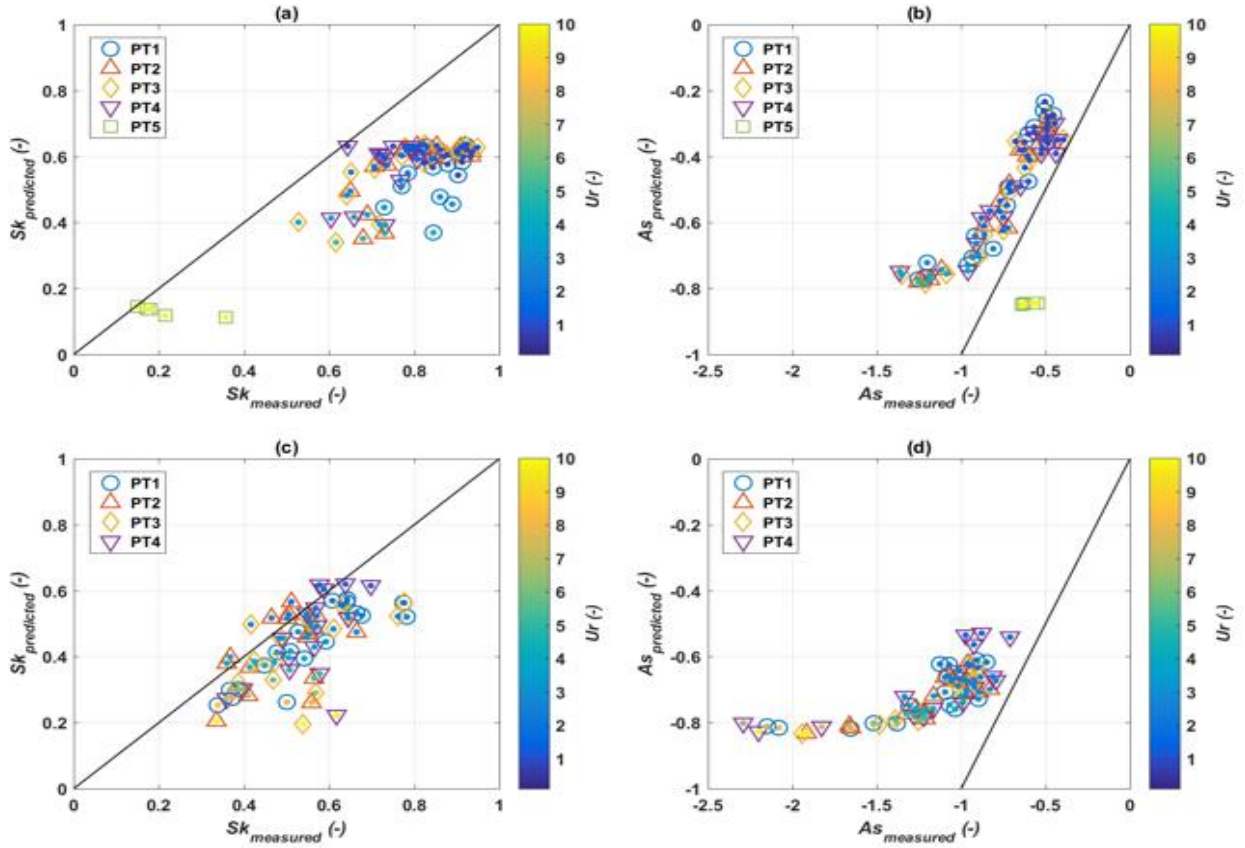

Figure 6 - Wave skewness (panels (a) and (c)) and wave asymmetry (panels (b) and (d)) measured values (x-axis) plotted against those predicted by Ruessink et al. (2012) parameterization (y-axis). Top panels (a) and (b) correspond to the first day of the field campaign. Bottom panels (c) and (d) are those of the second day of the experiment. In all four panels (a)-(d) the colour of each dot is set do display its respective Ur value (indicated in the vertical colour bar) and the symbols distinguish PT (according to the legend). Black lines indicate where measured (x-axis) and predicted (y-axis) nonlinearity are equal.

The trend in the *As* results is different (**Fig.6**, panels (b) and (d)). It is in the first day (panel (b)) that the parameterization performs better. In both days the higher *As* (absolute) and U_r values are associated to the worst fitting. This behaviour is more noticeable in the second day (panel (d)), with both U_r and $As_{measured}$ increase in response to the more energetic offshore conditions (and surf zone widening, as PT were located further inside the surf zone). Herein, it is evident how the *As* increase cannot be described by the ***R12*** formulation, in particular for the higher U_r values. $As_{predicted}$ (absolute value) seems to converge to 0.8 as measured asymmetry ($As_{measured}$) grows, once again suggesting a clear limitation in ***R12*** formulas concerning maximum nonlinearity values (both *Sk* and *As*). In fact, *As* maximum values underestimation showed to be even more pronounced (when compared to *Sk*) as ***R12*** formula underestimated measured *As* (maximum) values by ~50% and ~65%, respectively in the first (**Fig.6b**) and second (**Fig.6d**) days of the field campaign.

To investigate evidenced limitations in ***R12*** parameterization, **Fig.7** was drawn to display both the nonlinearity parameter (*B*) (panels (a) and (c)) and phase (ψ) (panels (b) and (d)) measured in the field against those estimated by ***R12*** formulas. In agreement with the discussed results of **Fig.6**, the formulation evidences a clear inability to estimate the higher values of the measured total nonlinearity ($B_{measured}$). In the first day (panel (a)), although with some scatter, *B* is fairly described to moderate values of measured total nonlinearity ($0.5 < B_{measured} < 1$). In turn, for the second day data (panel (c)), the formula performs well until relatively higher $B_{measured}$ ($B_{measured}$ ~ 1.2) suggesting the parameterization of ***R12*** to achieve better results in the description of waves nonlinearity in the second day of data recordings. (associated to higher energetic conditions). This trend is also evidenced to apply to the phase ψ. In the second day ψ exhibits a good agreement, as opposed to the first day where a considerable scatter is visible.

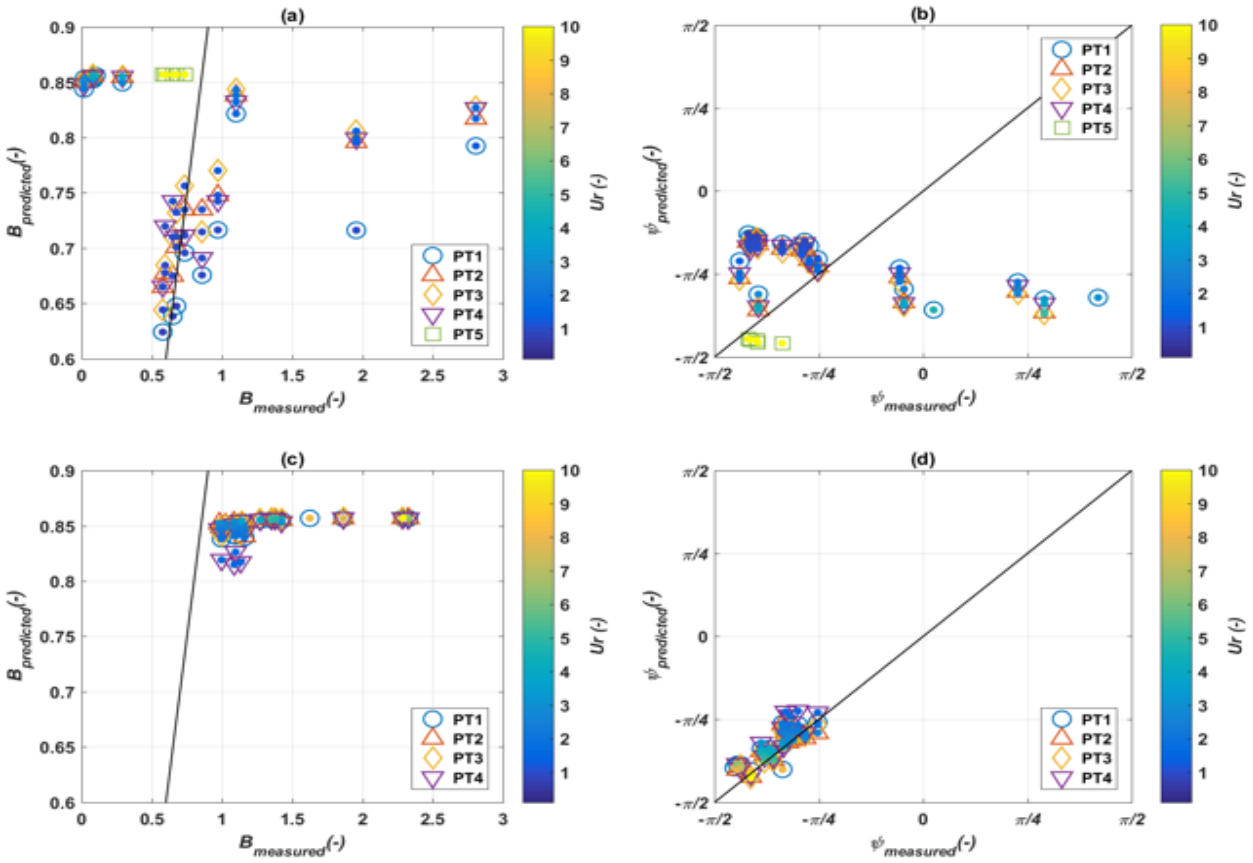

Figure 7 - Nonlinearity parameter (panels (a) and (c)) and phase (panels (b) and (d)) measured values (x-axis) plotted against those predicted by Ruessink et al. (2012) parameterization (y-axis). Top panels (a) and (b) correspond to the first day of the field campaign. Bottom panels (c) and (d) are those of the second day of the experiment. In all four panels (a)-(d) the colour of each dot is set do display its respective Ur value (indicated in the vertical colour bar) and the symbols distinguish between PT (according to the legend). Black lines indicate where measured and predicted values are equal.

Overall, the general nonlinearity underestimation provided by ***R12*** formulation is shown to be linked to the total nonlinearity parameter *B*, evidenced in **Fig.17c**. Note that as the phase ψ is accurately estimated, even for the higher U_r values, *B* becomes less precise with U_r increasing. In both days of the field experiment B_{max} is largely underestimated (~70% and 60%, respectively in day 1 and day 2), as opposed to the phase parameter (ψ), which is significantly well estimated in day 2 (**Fig.7d**) but shows a great scatter in day 1 (**Fig.7b**) of the experiment.

Of interest and once again, nonlinearity measures of the landward-most PT5 (which can only be found in panels (a) and (b), respective to the first day of the field campaign, in both **Fig.6** and **7**) are generally better predicted than those of the other PT. It is then possible that the steep bed slope in this specific cross-shore location (PT5) "forced" nonlinearity measures to be closer to nonlinearity simulations. For instance, notice that *As* (**Fig.6b**) is overestimated, contrarily to results exhibited in PT1 to PT4. Also, notice that the parameterization adjustment worsens, further underestimating *B* values as U_r increases. In contrast to this, it slightly overestimates *B* values corresponding to PT5. Hence, it may be possible that the sudden bed slope increase towards the cliff-foot is responsible for this odd shift in the parameterization performance. In fact, these results agree with those of *Rocha et al. (2017)*, who argued steeper bed slopes to restrict wave nonlinearity development (particularly B_{max}).

R12 parameterization curves are depicted in **Fig.8** to gain further insight. Results of nonlinearity measured in the field (represented by the circles) and estimated by the curves (represented by the lines) are plotted against U_r. Also, nonlinearity measured are set to display their respective values in terms of the local nondimensional parameter *kh*. In fact, this local parameter was reported to correlate to the ***R12*** formulation performance (*Rocha et al., 2013*).

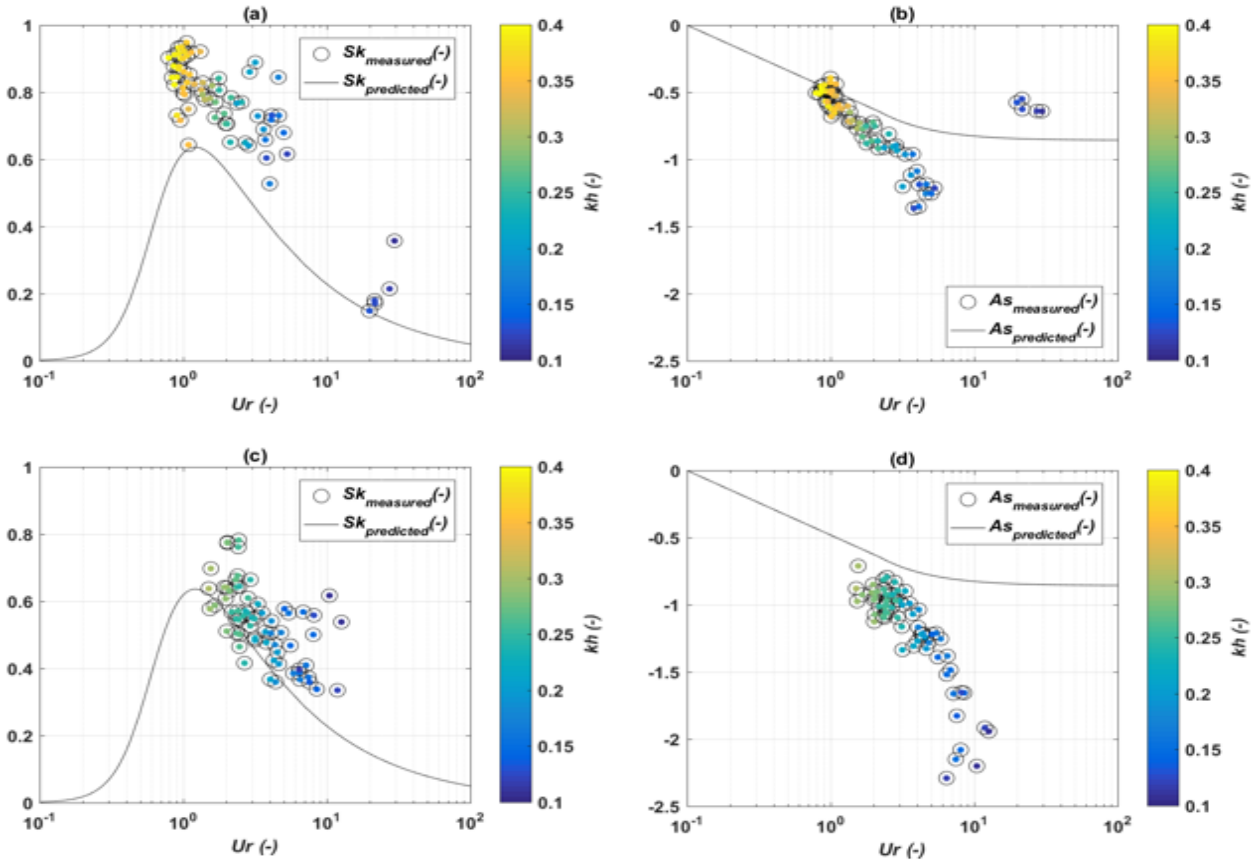

Figure 8 - Wave skewness (panels (a) and (c)) and wave asymmetry (panels (b) and (d)) measured values and those predicted by Ruessink et al. (2012) parameterization (y-axis, according to the legend) plotted against the Ursell number (x-axis, defined after Doering and Bowen (1995)). Top panels (a) and (b) correspond to the first day of the field campaign. Bottom panels (c) and (d) are those of the second day of the experiment. In all four panels (a)-(d) the colour of each circle is set do display its respective kh (~h/L) value (indicated in the vertical colour bar).

In terms of *Sk*, **Fig.8** (panels (a) and (c)) demonstrate that its variability trend is very well simulated. Despite underestimating *Sk* maximum values (more noticeable in the first day, panels (a)), the ***R12*** formulation curve seems to follow *Sk* variation (notice, that a vertical shift would be sufficient to accurately simulate the $Sk_{measured}$ maximum values). In the second day (panels (c)), because of the surf zone widening (due to the more energetic conditions registered), waves started to break in a seaward position relative to the PT positions.

Regarding *As* (panels (b) and (d)) it is obvious that, overall, the parameterization curve is far from providing precise results (except for $1 < U_r < 3$, in the first day (panel (b))). It can be inferred that it is for the second day of the field campaign (panel (d)) that ***R12*** formula deviated the most from the measured *As*. Although fairly describing *As* at $U_r \sim 1$, it completely fails to estimate *As* both values and trend as U_r increases (in contrast to panel (b)).

It it is for the lower *kh*, hence long waves and reduced depths (see the blue coloured dots in **Fig.8**) that the formula provided the worst underestimated results (**Fig.8b** and **8d**). These results comply with those of *Rocha et al. (2013)*, who established ***R12*** wave nonlinearity parameterization to provide less precise results for lower *kh* values, correspondent to the inner surf zone.

It is important to stress out that, herein, wave nonlinearity (in terms of both *Sk* and *As*) were estimated from surface elevation records, as opposed to the work of ***R12*** in which orbital velocity records provided the means to their wave nonlinearity estimations. *Poate et al. (2018)* have recently tested ***R12*** formulations with their own set of data, using measured surface elevation records and not velocity time series. Although the qualitative trend of both *Sk* and *As* evolution showed to be well descripted, *Poate et al. (2018)* reported the same overall *Sk* underestimation (more pronounced for increasing U_r values). However, in contrast to the present study, *As*

formulation provided an overall good fit to their data.

In this study, *Sk* maximum measured values are likely to have happened near the breaking point, after waves endured substantial shoaling (~ 25-30% underestimation). Although the overall *Sk* underestimation reported by *Poate et al. (2018)* can also be observed in our data (e.g., **Fig.6**), which may be linked to the different methodologies adopted in the wave nonlinearity estimation (i.e., near bottom pressure records vs near bottom orbital velocity records), ***R12*** parameterization completely failed to estimate maximum nonlinearity values in this study. In particular, *As* formula provided the worst results with the relative wave length decreasing ($kh \rightarrow 0$, **Fig.8b** and **8d**) (~ 50-65% underestimation).

4. CONCLUSIONS AND FUTURE RESEARCH

In the first day of data recordings *γ* displayed an upper bound value of 0.40, increasing to 1.00 at the landward-most position, highlighting the bottom slope influence on wave energy dissipation in the nearshore. Conversely, in the second day of the field campaign, the upper bound *γ* limit showed a slight increase to 0.51 that might indicate a response to a 30º shift of the offshore (frequency integrated) mean wave direction.

The comparison of the values of *Sk* and *As* indicate that the PT were located further inside the surf zone during the second day (i.e. *Sk* value decrease and *As* value was more negative) due to the more energetic wave conditions experienced. Furthermore, an apparent control of the bottom slope on *Sk* and *As* was identified in this analysis.

Measured *Sk* and *As* were compared with simulations provided by *Ruessink et al. (2012)* formulation. An overall underestimation was observed, enhanced for the higher U_r values. Maximum wave nonlinearity in terms of *Sk* was underestimated by 30-25% (respectively in the first and second days of the field campaign). However, it was for the *As* formulation that the estimations deviated the most from the measured values. In fact, a 50-65% underestimation was present for the maximum *As* measured values (respectively in the first and second days of the experiment). The above-mentioned underestimation showed to be linked to the total nonlinearity parameter (*B*).

Ruessink et al. (2012) formulation showed mixed results when applied to our data. The general wave nonlinearity underestimation trend may be explained by the different methodologies adopted to calculate both *As* and *Sk*, since these authors collected near bottom orbital velocity data, as opposed to the present work where near bottom pressure records were measured. However, maximum predicted values completely fail to adjust to our data. This is particularly evident for for the lower *kh* values (correspondent to the inner surf zone), to which the formulation provided the most inadequate results.

Apparently, both the offshore wave conditions and the bottom slope exerted specific controls on the parameterization performance, suggesting that the local parameters are not sufficient to achieve a fulfilled nonlinearity description. Although the qualitative trends of *Sk* and *As* can be well portrayed, enhanced shoaling (triggered by both low offshore wave steepness and bottom slopes, as waves are “allowed” to propagate further into the nearshore without breaking) and highly asymmetric (inner surf zone) waves could not be properly simulated by the parameterization formulas.

To the purpose of achieving an accurate wave nonlinearity description future researches shall improve the formulations tested herein (and others like those of *Rocha et al. 2017)*) by including field data collected both in inner and outer surf zone parts.

Acknowledgements
Umberto Andriolo and the whole team of the Faculdade de Ciências da Universidade de Lisboa are acknowledged for making available the field measurements, which they have carried out.

REFERENCES

Andrade, C., Marques, F., Freitas, M. C., Cardoso, R., & Madureira, P. (2002). Shore Platform Downwearing and Cliff Retreat in the Portuguese West Coast. *Litoral 2002, The Changing Coast, EUROCOAST/EUCC*, (January), 423–431.

Banner, M. L., & Phillips, O. M. (1974). On the incipient breaking of small-scale waves. *Journal of Fluid Mechanics*, *4*, 646–656.

Doering, J. C., & Bowen, A. J. (1995). Parametrization of orbital velocity asymmetries of shoaling and breaking waves using bispectral analysis. *Coastal Engineering*, *26*, 15–33.

Elgar, S., & Guza, R. T. (1985). Shoaling gravity waves: comparisons between field observations, linear theory, and a nonlinear model. *Journal of Fluid Mechanics*, *158*, 47–70.

Kennedy, A. B., Chen, Q., Kirby, J. T., & Dalrymple, R. A. (2000). Boussinesq modelling of wave transformation, breaking, and runup. *Journal of Waterway, Port, Coastal and Ocean Engineering*, 127(1), 39–47

Nairn, R., Roelvink, J., & Southgate, H. (1990). Transition zone width and implications for modeling surfzone hydrodynamics. In *Coastal Engineering Proceedings* (22).

Poate, T., Masselink, G., Austin, M. J., Dickson, M., & McCall, R. (2018). The Role of Bed Roughness in Wave Transformation Across Sloping Rock Shore Platforms. *Journal of Geophysical Research: Earth Surface*, *123*(1), 97–123.

Rocha, M., Silva, P., Michallet, H., Abreu, T., Moura, D., & Fortes, J. (2013). Parameterizations of wave nonlinearity from local wave parameters: a comparison with field data. *Journal of Coastal Research*, *65*, 374–379.

Rocha, M. V. L., Michallet, H., & Silva, P. A. (2017). Improving the parameterization of wave nonlinearities – The importance of wave steepness, spectral bandwidth and beach slope. *Coastal Engineering*, *121*, 77–89.

Ruessink, B. G., Ramaekers, G., & van Rijn, L. C. (2012). On the parameterization of the free-stream non-linear wave orbital motion in nearshore morphodynamic models. *Coastal Engineering*, *65*, 56–63.

Sallenger, A. H., & Holman, R. A. (1985). Wave energy saturation on a natural beach of variable slope. *Journal of Geophysical Research*, *90*, 11939–11944.

Sunamura, T. (1992). *Geomorphology of Rocky Coasts. Chichester, John Wiley & Sons*.

Thornton, E. B., & Guza, R. T. (1982). Energy saturation and phase speeds measured on the natural beach. *Journal of Geophysical Research*, *87*(C12), 9499–9508.